ELSEVIER

Astroparticle Physics 15 (2001) 149–165

Astroparticle Physics

www.elsevier.nl/locate/astropart

Time structure of the extensive air shower muon component measured by the KASCADE experiment

KASCADE Collaboration

T. Antoni [a], W.D. Apel [a], A.F. Badea [b], K. Bekk [a], K. Bernlöhr [a,1], H. Blümer [a,c], E. Bollmann [a], H. Bozdog [b], I.M. Brancus [b,*], A. Chilingarian [d], K. Daumiller [c], P. Doll [a], J. Engler [a], F. Feßler [a], H.J. Gils [a], R. Glasstetter [c], R. Haeusler [a], W. Hafemann [a], A. Haungs [a], D. Heck [a], T. Holst [a], J.R. Hörandel [a,2], K.H. Kampert [a,c], J. Kempa [e], H.O. Klages [a], J. Knapp [c,3], D. Martello [a,c], H.J. Mathes [a], H.J. Mayer [a], J. Milke [a], D. Mühlenberg [a], J. Oehlschläger [a], M. Petcu [b], H. Rebel [a], M. Risse [a], M. Roth [a], G. Schatz [a], F.K. Schmidt [a], T. Thouw [a], H. Ulrich [a], A. Vardanyan [d], B. Vulpescu [b], J.H. Weber [c], J. Wentz [a], T. Wiegert [a], J. Wochele [a], J. Zabierowski [f], S. Zagromski [a]

[a] *Institut für Kernphysik, Forschungszentrum Karlsruhe, 76021 Karlsruhe, Germany*
[b] *Institute of Physics and Nuclear Engineering, 7690 Bucharest, Romania*
[c] *Institut für Experimentelle Kernphysik, Universität Karlsruhe, 76021 Karlsruhe, Germany*
[d] *Cosmic Ray Division, Yerevan Physics Institute, Yerevan 36, Armenia*
[e] *Department of Experimental Physics, University of Lodz, 90236 Lodz, Poland*
[f] *Soltan Institute for Nuclear Studies, 90950 Lodz, Poland*

Received 11 May 2000; received in revised form 10 August 2000; accepted 12 September 2000

Abstract

The temporal structure of the extensive air shower (EAS) muon component ($E_{\text{thres}} = 2.4$ GeV) is studied at sea level by measurements of the muon arrival time distributions using the muon detection facilities of the KASCADE central detector. Data have been analysed for EAS core distances up to 110 m for primary energies around the knee region. The time structure of the EAS muon component is represented by the distributions of the mean, median, first quartile and the third quartile of the muon arrival time distributions relative to the foremost muon. The EAS time profiles (variation with the distance from the EAS center) are studied along their dependencies on the angle of incidence and the energy-indicative muon number N_{μ}^{tr}. Effects of the fluctuation of the arrival time of the first registered muon are scrutinised and corrected. The experimental results are compared with EAS Monte Carlo (CORSIKA–GEANT) simulations, fully

* Corresponding author.
E-mail addresses: iliana@muon2.nipne.ro (I.M. Brancus), rebel@ik3.fzk.de (H. Rebel).
[1] Present address: University of Hamburg, Hamburg.
[2] Present address: University of Chicago, Enrico Fermi Institute, Chicago, IL 60637, USA.
[3] Present address: University of Leeds, Leeds LS2 9JT, UK.

PII: S0927-6505(00)00148-1

including the detector responses and illustrating the phenomenological features. The comparisons, though generally in fair global agreement, revealed that the simulations underestimate the shower thickness and show nearly no dependence on the mass composition if the time resolution of the apparatus is realistically taken into account.

PACS: 96.40.Pq; 96.40.Tv
Keywords: Cosmic rays; Air shower; Arrival time distribution

1. Introduction

The particles of extensive air shower (EAS) move nearly in the direction of the primary particles with velocities close to the velocity of light. Transverse momenta of particles emitted in strong interactions and multiple scattering in the air produce a lateral dispersion. Differences in the velocities (''Lorentz effects'') and, in particular, in the path lengths, when travelling through the atmosphere, are the origin of a longitudinal dispersion (thickness) of the shower disk and of time delays of the arrival of the shower front, approximately represented by the relative arrival time of the first particle, relative to the arrival time of the core. The EAS thickness is manifested by the variation of the arrival times of particles, observed at a particular fixed location of the EAS lateral extension while the variation of the delays with the distance from the shower centre reflects the shape (curvature) of the EAS front and the direction of the incidence.

Linsley et al. [1,2] and Thielert and Wiedecke [3] systematically explored the lateral dependence of the shower thickness, expressed by the median delay time relative to the arrival time of the shower core. An increase of the time dispersion with the distance from the shower centre has been found. Since these early studies the time structure of the charged particle/photon component has been experimentally studied under various aspects. Walker and Watson [4,5] directed the interest to the time spread of the shower disk, whose origin could be interpreted as fluctuations of the height of maximum of the shower development due to different masses of the primaries, as consequence of different interaction lengths of the primaries and the multiplicities, energy and momentum distributions of the secondaries [6]. Most recently, Agnetta et al. [7] and Ambrosio et al. [8,9] presented detailed results on the temporal structure of EAS charged particles based on measurements with the GREX/COVER-PLASTEX set-up [7].

Simple kinematics arguments [10–13] show that the time spread, in particular of the muon component carries some information about the height of production i.e. the longitudinal EAS profile, via the time-of-flight effects. This feature arises from the fact that high-energy muons above a few GeV travel through the atmosphere in a relatively undisturbed way. The aspect has been pursued by detailed investigations of the temporal structure of the muon component with the Chacaltaya air shower array [14] and with a set-up of lead shielded liquid scintillators of the Haverah Park experiment by Blake et al. [15]. They explored the dependence of the time delay on the inclination θ of the shower axis, on the primary energy E_0 (or shower sizes N_e and N_μ), and on the distance R_μ from the shower core.

This specific kind of EAS investigations considers suitable shower observables which represent the arrival time distributions, e.g., the distributions of various characteristic quantities like mean values, median values of the individual distributions etc. and their dispersions. The variation of the mean of these quantities with the distance from the shower core R_μ represents the EAS time profile [16]. It depends on the energy E_0, the mass M of the primary particle (reflected by suitable shower variables like N_e, N_μ), on the zenith angle θ of shower incidence and additionally on biasing trigger and observation conditions: energy threshold E_{thres} and multiplicity n of the muon detection. Knowing the time profile may thus help to identify the primary particle and improve the energy determination.

The present experimental studies of the time structure of the EAS muon component are based on data measured with the KASCADE detector system [17–19]. The investigation explores phenomenological features, and studies empirical parameterisations of the observed time profiles, rather than the specific sensitivity to the mass of the primary particles. The experimental results are compared with results of detailed EAS Monte Carlo simulations, using the program CORSIKA [20,21] and taking into account the response and timing qualities of the detectors.

2. The timing and muon identification facilities of the KASCADE central detector

The KASCADE field covers an array of 252 detector stations, measuring the EAS electron–photon and muon components with a threshold of 5 and 230 MeV, respectively (for details see Refs. [17,18]). The central detector [22] (Fig. 1) is composed of several different detector components. Basically the set-up is an iron sampling calorimeter to identify hadrons and to measure their energy, position and angle of incidence, in particular in the shower core. Eight active detector layers measure the energy loss of the traversing hadrons in ionisation chambers. In the basement of the set-up there is an installation of large area position sensitive multiwire proportional chambers (MWPC) for the identification of muons of energies larger than 2.4 GeV [23]. They exploit the relatively good spatial resolution to study the lateral distribution of particles penetrating through the absorber above [24]. The MWPC system is arranged in double layers with a telescope effect, improving the reconstruction quality of the particle hits and giving information about the mean direction. Below the third iron layer, at a depth of $30X_0$ and with a mean energy threshold for muons of 490 MeV, plastic scintillators provide a fast trigger signal [25] and are used for timing measurements. This timing layer is composed of 456 detector elements, covering effectively 64% of the total central detector area of 16×19 m^2. Each detector consists of two quadratic scintillator sheets of 3 cm thickness and 0.45 m^2 in total area, with a readout by a wavelength shifter bar and an 1.5-in. photomultiplier. Two of these elements are housed, optically separated, in a light-tight detector box. The average time resolution has been determined to be 1.7 ns. In addition, this detector layer is used as $\mathrm{d}E/\mathrm{d}x$ detector for (muons and other) charged particles ($E_{\mathrm{thres}} = 0.49$ GeV). Two different thresholds of the electronic readout allow to discriminate the energy loss of minimum-ionising particles (m.i.p.) and of hadrons (50 m.i.p.) [25]. The contribution of punch-through events of the electromagnetic component to muons events, identified with the low-energy threshold, becomes negligible for distances >30 m from the shower centre. For studies of the high-energy muons a correlated measurement of the MWPC and the trigger layer detectors is performed. Due to the good angular resolution of the MWPC (<1° for $E_\mu > 10$ GeV) it is possible to use them to identify high-energy muons. For filtering, every

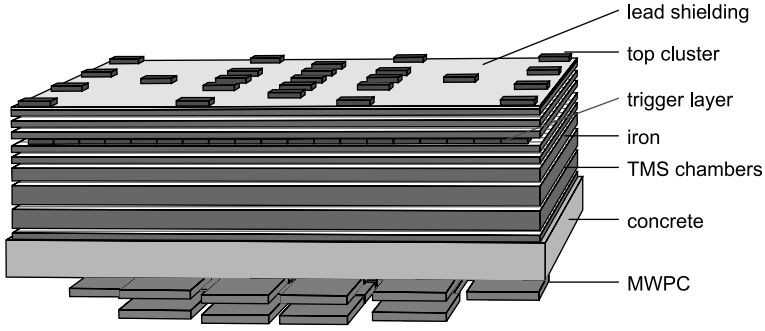

Fig. 1. Sketch of the KASCADE central detector.

reconstructed muon is traced back through the central detector up to the trigger layer. In case that the track is hitting a trigger detector with a valid signal the time is used for further analysis. With this procedure one is able to suppress efficiently the low energy muons. The MC simulations show that about 75% of the 2.4 GeV muon tracks in the MWPC have a correlated signal in the trigger layer. This corresponds to the coverage of the trigger layer of the active area of the MWPC. On the other hand only about 26% of the trigger detectors have a correlated signal with the MWPC. This is smaller than the active area (43%) of the MWPC. The central detector system allows to study lateral and time distributions of the muon component with two different energy thresholds [26].

3. General procedures

3.1. Definition of the observables

The present investigation explores the temporal features of the muon component of EAS events at muon energies above 2.4 GeV. An event can be characterised by the shower core position R_{cor} e.g., measured from the centre of the central timing layer, the direction of shower incidence (with the zenith angle θ and azimuth angle Φ), by the shower size N_{e}, the muon number N_{μ} or the "truncated" muon number N_{μ}^{tr}. The quantity N_{μ}^{tr} is the number of muons with $E_{\mu} \geqslant 230$ MeV, integrated in a limited range of 40–200 m from the shower centre. As Monte Carlo simulations show [27,28], due to various fortunate features of the lateral distribution, $\log_{10} N_{\mu}^{\mathrm{tr}}$ proves to be nearly proportional to $\log_{10} E_0$ and is almost independent of the primary mass at the KASCADE observation level. Therefore, we prefer a classification according to N_{μ}^{tr} instead of the shower size N_{e}. The latter would prepare samples of mixed energies, dominated by proton-induced showers [24]. For showers located within 90 m from the array centre, the reconstruction accuracy is about 3 m for the location of the shower centre, 0.5° for the angle of incidence and 10–20% for N_{e} and N_{μ}^{tr}.

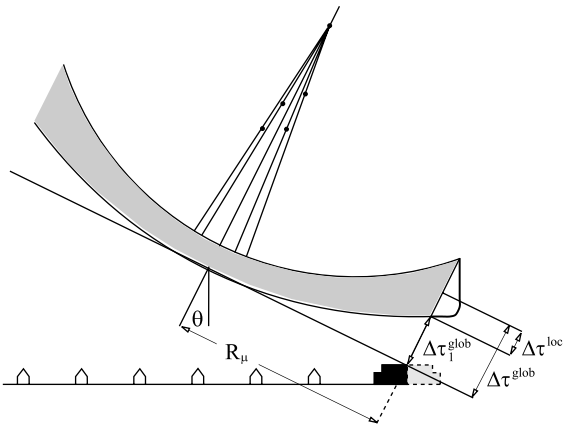

Fig. 2. Characterisation of the EAS temporal structure by global and local arrival times.

Measurements of the relative muon arrival times refer to an experimentally defined zero time (Fig. 2). In many studies the arrival time of the shower core τ_{cor} has been used as reference [11–13], also in the first analysis of relative muon arrival times with KASCADE data [29]. In that analysis the distributions of the arrival time of the foremost muon $\tau_{1\mu}$, of the mean τ_{μ} of the single event distributions, and the corresponding standard deviations σ have been regarded:

$$\Delta\tau_1^{\mathrm{glob}}(R_{\mu}) = \tau_{1\mu}(R_{\mu}) - \tau_{\mathrm{cor}} \tag{1}$$

$$\Delta\tau^{\mathrm{glob}}(R_{\mu}) = \tau_{\mu}(R_{\mu}) - \tau_{\mathrm{cor}} \tag{2}$$

Time quantities referring to τ_{cor} are further on called "global" times. Experimentally, it turned out [29] that τ_{cor} is not well determined from the arrival time of the electromagnetic component near the shower core with the present reconstruction procedures, and it introduces an additional jitter of some nanoseconds. Hence, for the present studies we prefer to consider "local" times, which refer to the arrival of the foremost muon, registered in the timing detector at the particular distance from the centre $R_{\mu}(=R_{\mathrm{cor}}$ in case of vertical showers):

$$\Delta\tau^{\mathrm{loc}}(R_{\mu}) = \tau_{\mu}(R_{\mu}) - \tau_{1\mu}(R_{\mu}) \tag{3}$$

(The label "loc" is omitted further on.)

It should be immediately noted that the first detected muon does not well define the shower front. This approximation is mainly dependent on the multiplicity of the sample (taken from the particle population in the shower disk) and needs at low multiplicities a correction of the observed delay distribution with respect of the true arrival time distribution (see Section 3.4). In general, R_μ is defined in a plane perpendicular to the shower axis, which is specified by zenith angle θ and the azimuth angle Φ of the direction of incidence.

For a detailed discussion of the time structure we use specific quantiles $\Delta\tau_\alpha$ of the distributions, the *first quartile* ($\Delta\tau_{0.25}$), the *median value* ($\Delta\tau_{0.50}$) and the *third quartile* ($\Delta\tau_{0.75}$) which exhibit different features of the time structure of the muon component. For ordered statistics of measured times $\Delta\tau_1 \leqslant \Delta\tau_2 \leqslant \cdots \leqslant \Delta\tau_n$ and $k := n\alpha + \xi$, k integer and $\xi \in [0,1)$, the α-quantile $\Delta\tau_\alpha(\alpha \in (0,1))$ is the following [30]:

$$\Delta\tau_\alpha = \begin{cases} (\Delta\tau_k + \Delta\tau_{k+1})/2: & \text{for } \xi = 0 \\ \Delta\tau_k: & \text{for } \xi \in (0,1) \end{cases} \quad (4)$$

That means: in the case of large n, a fraction α of muons has arrival times less than $\Delta\tau_\alpha$.

3.2. Measurements

The experimental data have been accumulated in the period January 1998–April 1999 and the data sample comprises more than 3.4 millions of reconstructed showers. The EAS reconstruction procedures are described elsewhere [26]. For the arrival time analysis, at least three detectors of the trigger layer are required to have a signal which can be correlated with three muon tracks in the MWPC. Generally measurements of the muon component at small core distances could be affected by the electromagnetic punch through and by the hadrons in the shower core. Due to the selection of muons with $E_\mu \geqslant 2.4$ GeV by the MWPC positioned below the iron sampling calorimeter, a disturbance by electromagnetic punch through is found to be negligible. There are no deviations visible from the Landau distribution of the energy deposits of the identified muons, even at small $R_\mu = 10$ m [38]. But cascading hadrons systematically fake early "first muons" in the scintillation detector, which distort the relative arrival time distributions. In order to suppress muon signals faked by hadrons, a veto for a large energy deposit in the scintillator detectors $E_{\text{dep}} \geqslant 20$ MeV (c. 3 m.i.p.) has been applied. This procedure remedies the distortion effect in the shower centre as displayed in Fig. 4. Previous studies [31] have shown that by use of a cut on the arrival time of the first muon the analysis could be safely performed up to radii $R_\mu < 110$ m. In fact, the muon arrival times at large radii are of particular interest for mapping the time structure to production heights since the path-length effects become more pronounced [11,12].

3.3. EAS and detector response simulations

The observed muon arrival time distributions are compared with simulations of the air shower development, calculated with the Monte Carlo air shower simulation program CORSIKA (ver. 5.621) [20,21]. This program includes the GHEISHA code [32] and various packages of high-energy interaction models like VENUS [33] and QGSJET [34] as generators of the hadronic interactions. The electron–photon component is simulated by the EGS4 Monte Carlo procedure [35]. The influence of the Earth's magnetic field on the muon propagation has been taken into account. As density profile of the atmosphere the US standard atmosphere is chosen [20,21].

The actual calculations are based on the QGSJET model and cover an energy range of 5×10^{14}–3.06×10^{16} eV (divided in seven energy bins) and a zenith angle range of 0–40°. They are performed for three mass groups: H = light group, O = CNO group, Fe = heavy group with an energy distribution of a spectral index of -2.7. They comprise a set of $\simeq$2000 showers for each case, except for the bins of the highest energies (6.51×10^{15}–1.82×10^{16} eV with $\simeq$1000 simulated showers and 1.09×10^{16}–3.06×10^{16} eV with $\simeq$500 simulated showers). The response of the KASCADE detector system and the timing qualities have been simulated using a program, developed on the basis of the GEANT code [36]. The particles of the simulated EAS are tracked through

the detector set-up and the timing response of the detectors are recorded for various core distances from the central detector facilities. Particularly, it should be noted that the timing depends on the energy deposit in the scintillation detectors. This effect has been corrected by introducing an adequate procedure.

3.4. Multiplicity effects

The present studies consider time distributions relative to the arrival time of the foremost muon and with muon multiplicities $n \geqslant 3$. Fig. 3 displays the average single muon arrival time distribution as observed experimentally in the distance of 60–70 m from the shower core for $\simeq$2000 EAS events. In an event-by-event consideration intriguing statistical effects enter in the estimate of the properties (like the median) of the probability density function (p.d.f.) from small samples of muons. Following the considerations of Ref. [37] it can be shown that the arrival time $\tau_{1\mu}$ of the foremost muon (relative to a fictive time zero, representing the muon front and approximated with a sample of very large n), its fluctuations and the estimated median value, e.g. of $\Delta\tau^{\mathrm{loc}} = \tau_{\mu} - \tau_{1\mu}$ depend on the particular value of the multiplicity n, systematically increasing the mean values of the quantities with increasing n. The actual observed profiles are derived from samples $\tau_{1\mu}$, $\tau_{2\mu}$, ..., $\tau_{n\mu}$ of different muon multiplicities, with the average multiplicities depending on R_{μ} and decreasing with the core distance, for the case of different $\log_{10} N_{\mu}^{\mathrm{tr}}$ values differently, according to the lateral muon density distributions. For example, for $\log_{10} N_{\mu}^{\mathrm{tr}} = 4.0$–$4.25$ and 40 m $< R_{\mu} \leqslant 50$ m the mean value of the multiplicity $\overline{n}$ is about 16 with a distribution extending to $n \simeq 40$, while for the range 100 m $< R_{\mu} \leqslant 110$ m the value $\overline{n}$ is about 8. Thereby in the experiment we observe EAS events of different primaries, which exhibit different lateral muon densities and different arrival time distributions. This implies that the particular mixture of contributions of different EAS primaries to the observed arrival time distributions is also varying with R_{μ}. The effect that the arrival time of the foremost muon is deviating from the ideal shower front, fluctuating with the sample multiplicity is relatively small in the pure CORSIKA simulations. But it seriously distorts the experimental arrival time distributions as well as the simulated distributions, when the smearing due to the finite time resolution [38] is taken into account. Though in principle a comparison of the data could be made with simulations including the effect, we do prefer to remove the distortions arising from the measuring apparatus by an adequate correction procedure. Such an procedure by a "local time correction function" invokes EAS simulations and is described in Appendix A. The effect of the correction procedure is indicated in Fig. 4.

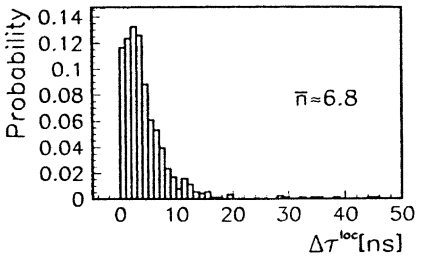

Fig. 3. Averaged single muon arrival time distribution observed at $R_{\mu} = 70$–80 m with $3.6 < \log_{10} N_{\mu}^{\mathrm{tr}} \leqslant 4.8$ (corresponding to 8×10^{14}–3×10^{16} eV) for the angular range $5° < \theta \leqslant 30°$.

4. The time profile of the EAS muon component

The experimental distributions of the quantiles are considered in different intervals of the core distance $R_{\mu} = 10$–20 m, up to 100–110 m, for zenith angles in different ranges from 0° to 40° and for five different N_{μ}^{tr} ranges.

4.1. Shape of the arrival time distributions

Simple kinematics arguments lead to a qualitative understanding of the gross shape of the arrival time distributions, which also imply a variation (broadening) with increasing distance from the shower centre. Fig. 5 compares the experimental and simulated muon arrival time distributions of different quantiles for the radial range of $R_{\mu} = 90$–100 m. At a first glance it displays a fair overall agreement between experimental and

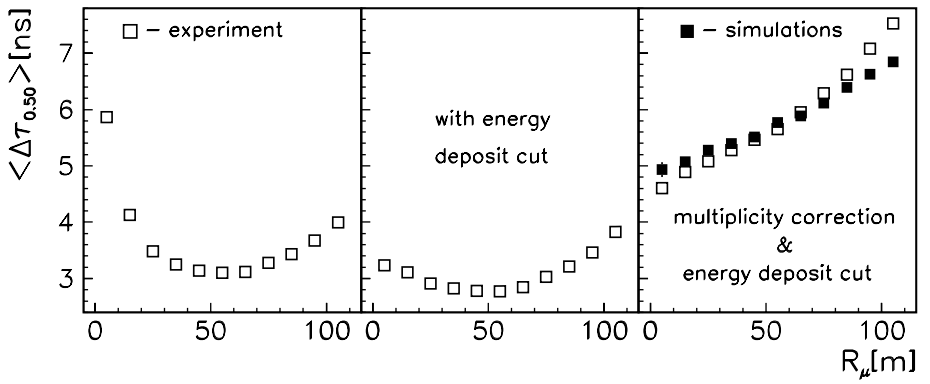

Fig. 4. Observed EAS median time profiles $\langle \Delta\tau_{0.50} \rangle$ for the sample with $3.6 < \log_{10} N_{\mu}^{tr} \leqslant 4.8$ for the angular range $5^{\circ} < \theta \leqslant 30^{\circ}$ without and with correction procedures applied. The corrected profile is displayed with EAS simulations.

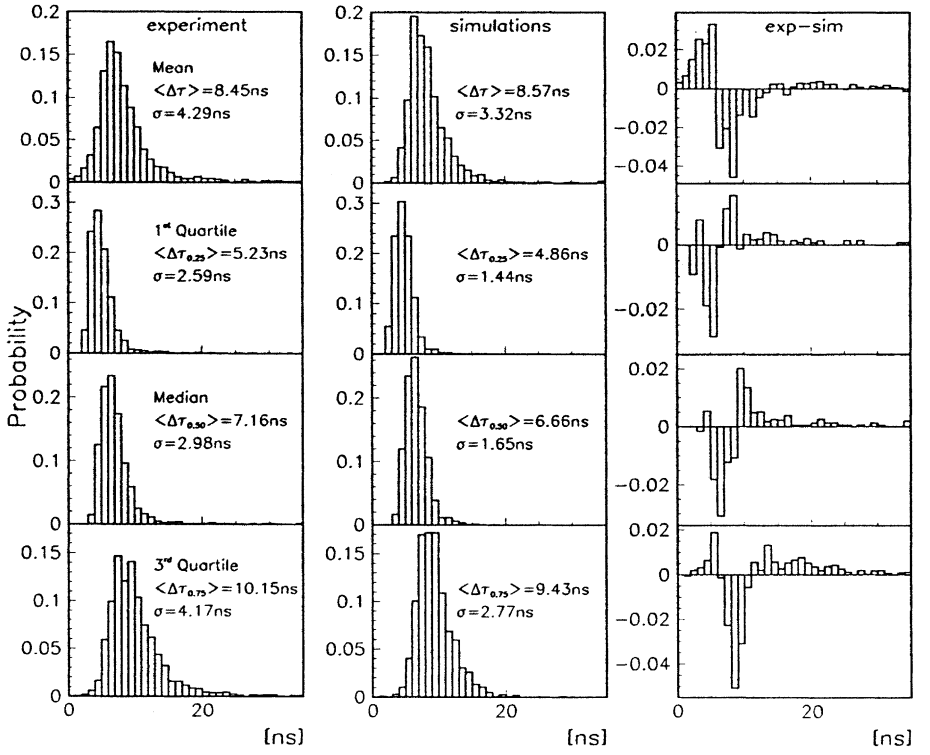

Fig. 5. Distributions of different time quantities for the particular sample with $4.25 < \log_{10} N_{\mu}^{tr} \leqslant 4.45$ for the angular range $5^{\circ} < \theta \leqslant 30^{\circ}$ and the radial range: 90 m $< R_{\mu} \leqslant 100$ m. The simulations adopt a mass composition: H:O:Fe = 4:1:2.

simulated data. For the simulations a mass composition suggested by Ref. [39] has been adopted, but other composition choices have been also considered and are shown to change only insignificantly the results [40]. The simulated mean muon arrival time and standard deviation values are smaller than the experimental ones. In both cases, the fast component ($\Delta\tau_{0.25}$) is narrower than

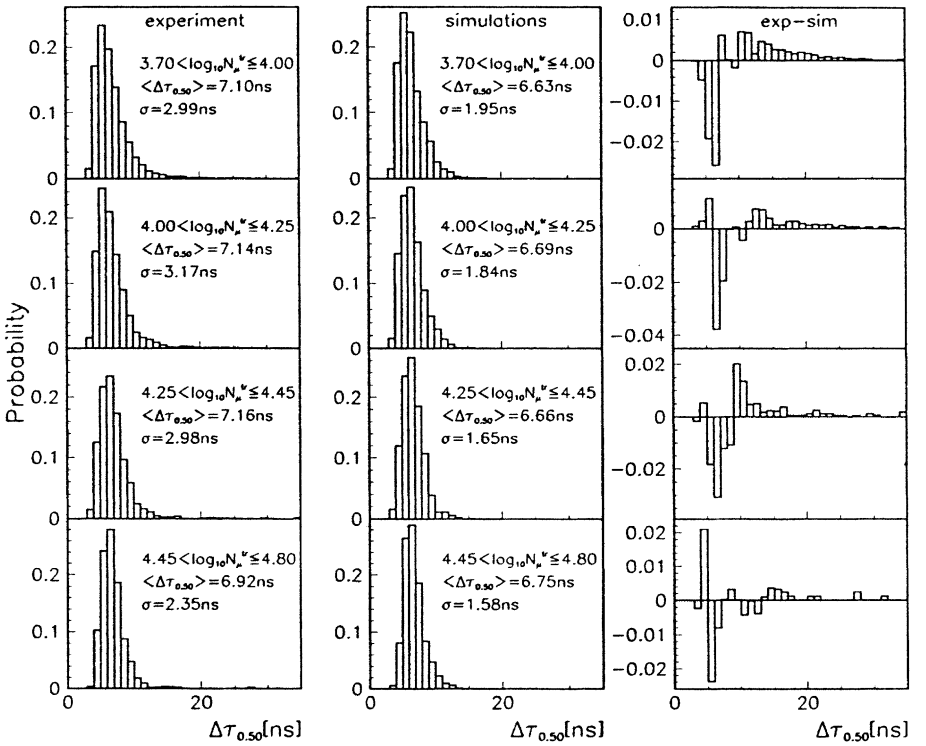

Fig. 6. Distributions of the median muon arrival time for different $\log_{10} N_{\mu}^{\mathrm{tr}}$ ranges displayed for the angular range $5° < \theta \leqslant 30°$ and the radial range: 90 m $< R_{\mu} \leqslant 100$ m. The simulations adopt a mass composition: H:O:Fe = 4:1:2.

the median ($\Delta\tau_{0.50}$), the latter suppresses the influence of large fluctuations affecting the mean ($\Delta\tau$). Fig. 6 presents the dependence of the experimental and simulated median time values on the N_{μ}^{tr} range (indicating the primary energy), exhibiting narrower distributions for higher energies. The data have been processed for all radial ranges by determining the mean values and the variances σ^2 (standard deviations of σ) of the mean ($\Delta\tau$), the median ($\Delta\tau_{0.50}$), and of the quartiles ($\Delta\tau_{0.25}$) and ($\Delta\tau_{0.75}$). Figs. 7 and 8 show the observed variations of the distributions of the quartiles ($\Delta\tau_{0.25}$) and ($\Delta\tau_{0.75}$) of the muon arrival time distributions with the distance from the shower core (for a particular N_{μ}^{tr} range). With increasing radial distances both types of distributions become broader and shifted to larger mean values of the local delay times (local profiles). In studies of the charged-particle EAS component [7] it has become customary to parameterise the observed distributions by a Γ p.d.f. [41,42] given by:

$$\Gamma(T) = a\,T^{b}\exp(-c\,T), \quad (T = \Delta\tau_{\alpha}) \tag{5}$$

with a mean value $\langle T\rangle = (1+b)/c$ and the standard deviation $\sigma_{\Gamma} = (1+b)^{1/2}/c$. We do not apply the parameterisation by the Γ-form as arising from a specific mathematical model of the EAS development, but it is empirically justified. It can be shown that the shape with a fast increase and a longer decreasing slope reflects just the gross longitudinal development of the muon component [16], but any other parameterisation of this type may be of similar convenience for fitting the bulk of data. Figs. 7 and 8 show as examples experimental and correspondingly simulated distributions fitted by the Γ-form (further examples are given in Ref. [40]). Only the tails of the experimental distributions are less well described by the Γ-form (Fig. 9). This feature of "delayed showers" has been noticed and stressed in the shape of the time distributions of the EAS charged particle component [8,9] and has been associated to fluc-

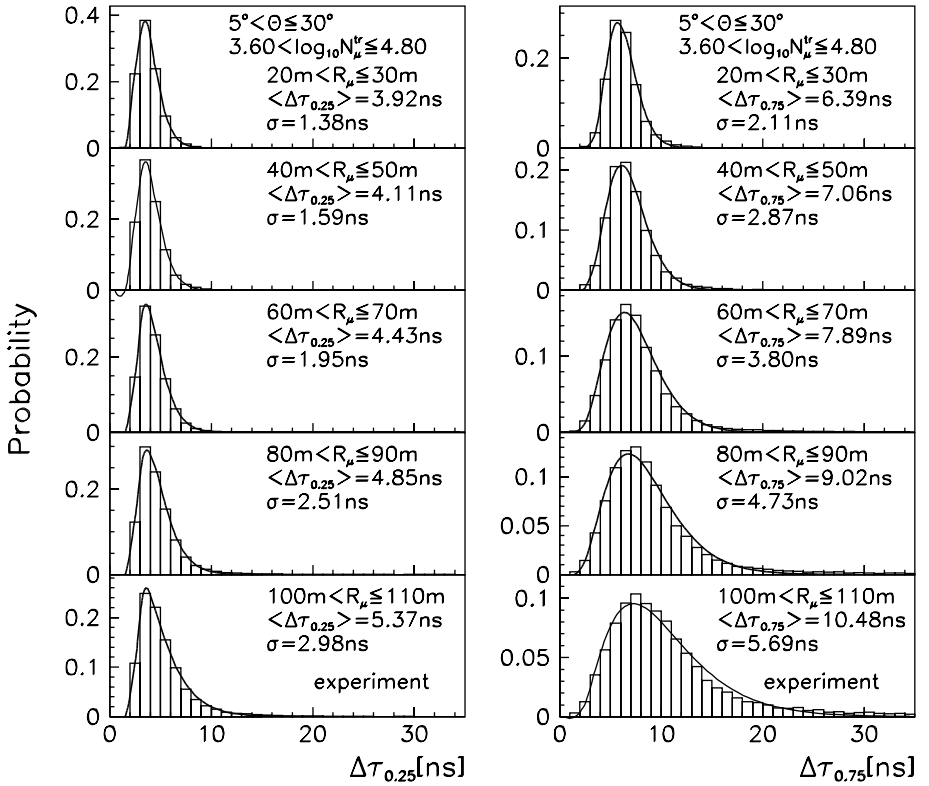

Fig. 7. The variation of the shape of the experimental distributions of the first and third quartiles with the core distance. The lines display fits by the Γ-form.

tuations of the shower development, insufficiently accounted for in the simulations. A considerable part of these "delayed" tails may be accounted to uncorrelated particles triggering the zero time too early. In our case the contribution arising from uncorrelated muons is estimated to be less than 20% of the observed excess in Fig. 9, and completely negligible for the total distribution at all. Nevertheless, we cannot follow the conclusions of Ref. [9] that these "delayed" tails are a specially interesting feature in the arrival time distributions. In fact, an alternative heuristic parameterisation by a logarithmic Gauss distribution [43] does sufficiently well reproduce such tails as pointed out by Battistoni et al. [44].

When comparing the variation of the experimental and simulated muon arrival time distributions for different N_μ^{tr} ranges, there appears a systematic tendency that the distributions of the simulated data underestimate the thickness of the muon disk. This feature is displayed in Fig. 10 showing the $\log_{10} N_\mu^{tr}$ dependence of the mean values (and their uncertainties) of the median and third-quartile distributions at two distances from the shower core. Like above the simulations are based on an adopted particular primary mass composition: H:O:Fe = 4:1:2, but the gross features do not depend very much on that. A particular feature, especially pronounced with the third quartile, is the tendency of a decreasing time spread of the local profile with increasing primary energy (N_μ^{tr}), roughly beyond the knee position ($\log_{10} N_\mu^{tr} \simeq 4.1$). The origin of this feature has not been explored in detail. The observation can be associated with the energy variation of the lateral muon contribution, i.e. with varying local contributions from different muon production heights, and thus of EAS induced by different kind of primaries. Since the simulations (with a fixed primary mass composition) exhibit similar features, a

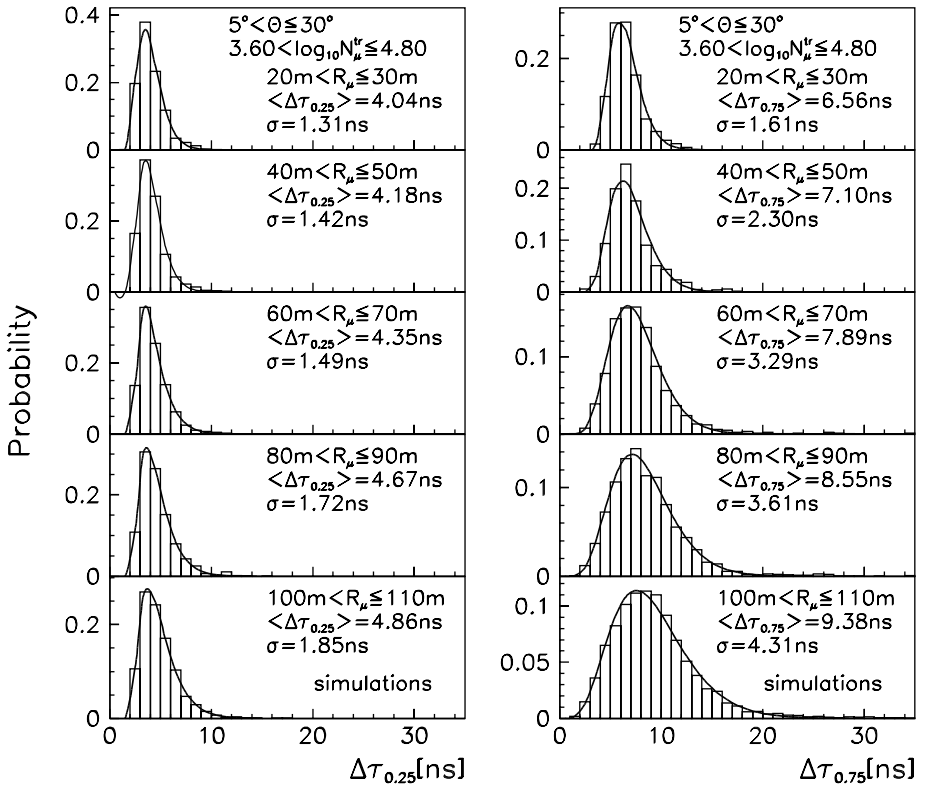

Fig. 8. Corresponding to Fig. 7 the variation of the shape of the simulated distributions of the first and third quartiles with the core distance. The lines display fits by Γ-form.

change of the mass composition with the primary energy cannot be considered to be a main reason of e.g. the decreasing spread of the third quartile. Fig. 11 displays the shapes of the median arrival time distributions for three different (broad) ranges of the EAS zenith angle and shows no significant variation. The decrease of the time dispersion of the local profile with the EAS age, shown for two ranges of R_μ (Fig. 12), may be qualitatively understood as the correspondence between age and the depth of the EAS maximum. It should be noted that Fig. 12 shows averages over the total N_μ^{tr} range which may explain the good agreement as compared to Fig. 10.

4.2. Time profiles

The R_μ-dependence of distributions of the various time quantities, or expressed in a more concise way, of the mean values and their dispersion (time profiles: $\langle\Delta\tau\rangle$, σ; $\langle\Delta\tau_{0.25}\rangle$, $\sigma_{0.25}$; $\langle\Delta\tau_{0.50}\rangle$, $\sigma_{0.50}$; $\langle\Delta\tau_{0.75}\rangle$, $\sigma_{0.75}$) represents the time structure of the EAS muon disk. Figs. 13 and 14 present experimental profiles for the time distributions for different N_μ^{tr} ranges and angular ranges of EAS incidence, respectively, and compare with EAS simulations. The uncertainty in the mean values and in the standard deviations, given by $\sigma/\sqrt{N}$ and $\sigma/\sqrt{2(N-1)}$, respectively, (N being the number of events) are indicated by the vertical bars (so far visible). In general a good overall agreement (except for larger R_μ) for the mean values can be noticed, while the variances appear distinctly smaller in case of the simulations. As compared to the total charge particle component [8] the width of the muon component is significantly smaller. This finding is in contrast to the conclusions of Ref. [8]. The shape of the EAS time profiles may be approximated by the form [7]:

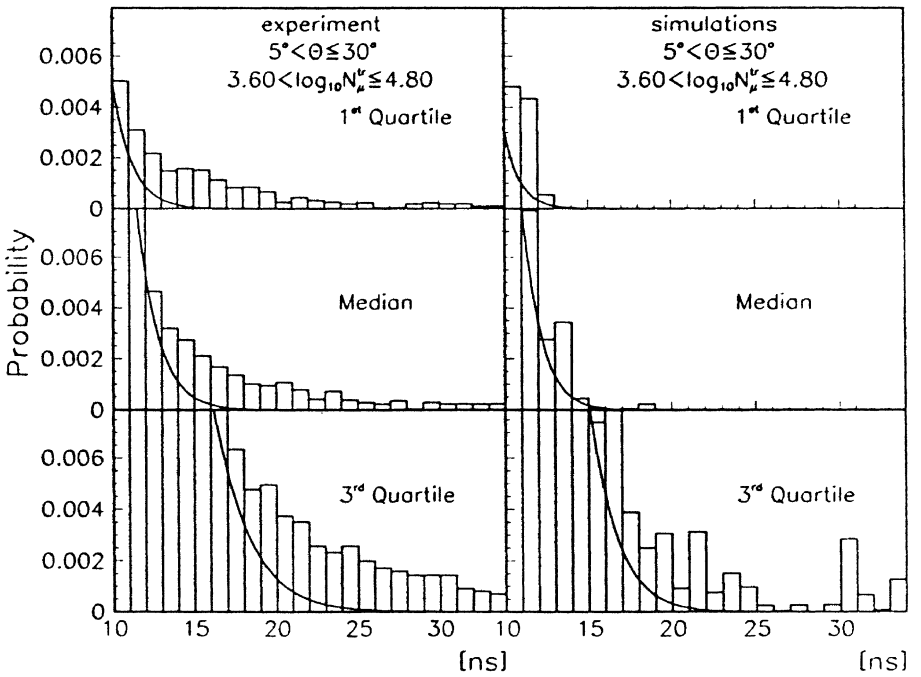

Fig. 9. Tails of the experimental and simulated distributions for various time quantities for 70 m $< R_\mu \leqslant$ 80 m, fitted with the Γ-form. The simulations adopt a primary mass composition: H:O:Fe = 4:1:2.

$$T(R_\mu) = t_1 + t_2(R_\mu/R_m)^\beta, \quad (T = \Delta\tau_\alpha) \tag{6}$$

with R_m the scaling radius for the muon lateral distribution function (determined for $E_\mu \geqslant 2.4$ GeV to be $R_m = 100$ m [45]). Such an empirical formula (whose parameters for the muon component have been determined for different dependencies on basis of a smaller data sample in Ref. [31]) accounts for the increasing width of the charge particle component at larger distances from the core. It was suggested [46] that a parameterisation of the observed feature could be used to determine the core location. At a closer look the muon component, whose time structure is different and with the muon disk walking ahead the electromagnetic component [47], shows some deviations from the quasi-parabolic shape ($\beta \simeq 2.0$). As obvious in Fig. 14, the variation of the profile with the EAS angle of incidence is relatively weak for the considered distances from the shower centre, though not completely negligible. It should be noted that because of lack of statistically equivalent samples of simulated events for inclined showers, for the sake of simplicity the multiplicity corrections have been done on basis of the correction function for vertical showers. This might affect the systematic accuracy of the results of Fig. 14, shown without simulations, which nevertheless reproduce the gross features of the observations (see also Fig. 6).

5. Concluding remarks and summary

The present paper studies the phenomenological features of the time structure of the EAS muon component ($E_\mu \geqslant 2.4$ GeV) based on experimental observations with the KASCADE detector. The investigations are focussed to observables characterising the time spread of the muon shower disk and its variation with the distance from the centre. For that purpose the local arrival time distributions of muons relative to the arrival time of the first registered muon are measured, event by

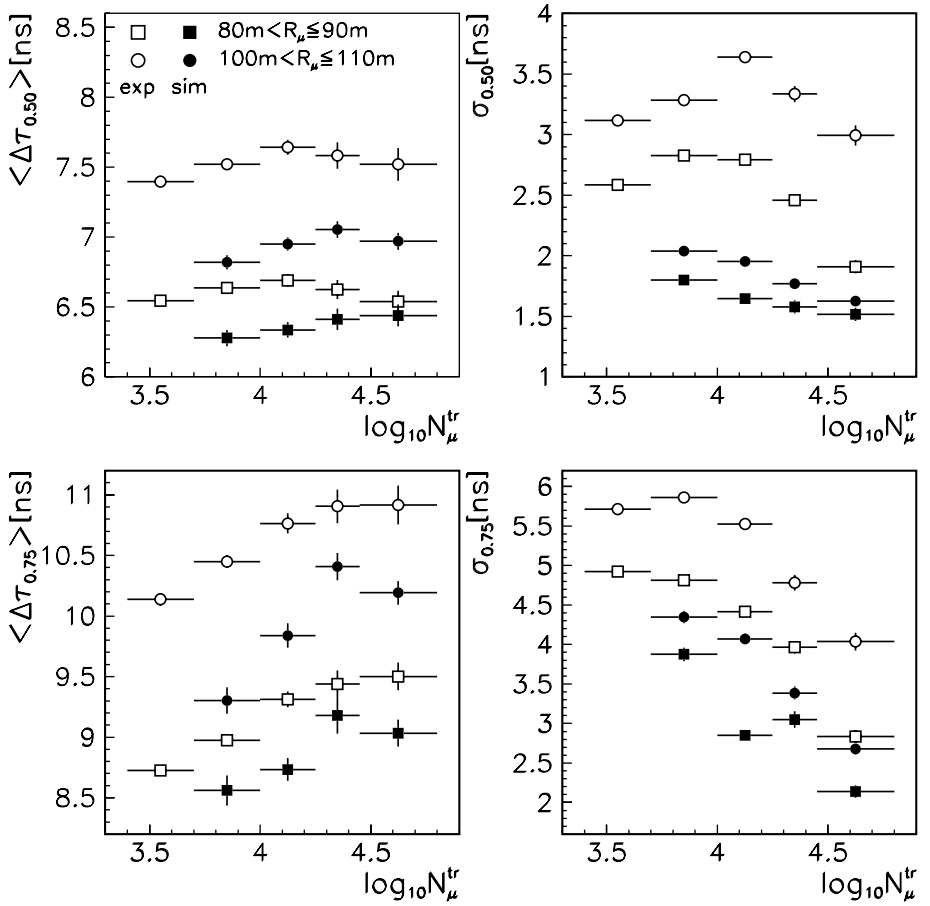

Fig. 10. Energy dependence of the mean values and their uncertainties of the experimental and simulated median and third-quartile distributions observed at two different ranges of the distance from the shower core ($5° < \theta \leqslant 30°$).

event and correlated with a number of other observables specifying the shower (N_e, N_μ^{tr}, age, ...). Various time parameters are inferred to characterise the single arrival time distributions: mean ($\Delta\tau$), median ($\Delta\tau_{0.50}$), first ($\Delta\tau_{0.25}$) and third ($\Delta\tau_{0.75}$) quartiles. Because of the relatively small number of muons (sample multiplicity) defining the observed single distributions, these quantities are subject of various fluctuations, in particular of the fluctuation of the arrival of the first muon used as zero calibration point. As compared with the time delay distributions determined with respect to the well-defined arrival of the light front in the shower core (''global'' arrival time distributions), this fluctuation leads to a noticeable dependence of the local characteristic quantities from the muon multiplicity of the sample, as discussed in Refs. [10,37]. Since the average multiplicity varies with the lateral distance from the EAS core, the observed local time distributions are superpositions for different multiplicities. Intriguing features arising from the effect that the time zero reference does not always reflect the extreme shower front, have already pointed out with KASCADE data in Ref. [31] and become more pronounced, when the finite time resolution of the detectors is taken into account. Hence, for a reasonable discussion of the arrival time distributions a correction procedure has been applied in the observed data as well as in the detector simulations, removing the experi-

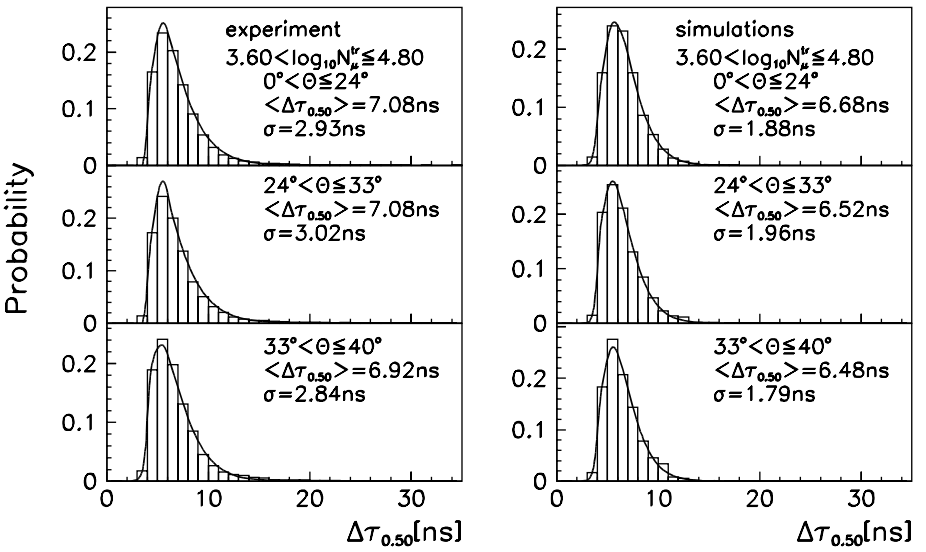

Fig. 11. Experimental and simulated median time distributions for three different angular ranges (equal sec θ – bins) of EAS incidence, fitted with the Γ-form (90 m $< R_\mu \leqslant$ 100 m). The simulations adopt a primary mass composition: H:O:Fe = 4:1:2.

mentally induced distortions by the fluctuations around the "true" reference point. The arrival time distributions exhibit following features:

(1) In general, there is a good overall agreement between the experimental distributions and the predictions by Monte Carlo simulations of the EAS development by the CORSIKA code, and it confirms that the code describes well observables sensitive to the longitudinal EAS development.

(2) The shapes of the experimental and simulated arrival time distribution can be sufficiently well described by a phenomenological parameterisation in terms of the Γ p.d.f., with some additional tails observed in the experimental distributions. But these tails are much less pronounced than observed with the charged particle distributions [7]. A closer look reveals a significant tendency that the theoretical distributions, based on a particular adopted primary mass composition, predict smaller time delays relative to the local front and a smaller spread of the muon disk, especially at larger distances R_μ from the EAS core. Nevertheless, the thickness of the muon disk ($E_\mu \geqslant 2.4$ GeV) is significantly smaller than of the electron component ($E_e \geqslant 4$ MeV). This finding is in disagreement to conclusions of the analysis of the GREX/COVER-PLASTEX experiment [8].

(3) Regarding the shower profiles the mean delays and the thickness are increasing with increasing R_μ, whereby the variation of the third-quartile distribution is more pronounced than of the first quartile. In agreement with analyses of Monte Carlo simulations, the variations, which show that the muon disk is flatter than that of electrons, can be fairly well approximated by a quasi-parabolic shape in the radial range close the EAS center up to $R_\mu = 110$ m. While the simulations reproduce even some deviations of the local mean delays from parabolic shape, which presumably reflect the original influence of varying sample multiplicities (also present in pure CORSIKA simulations), they underestimate the fluctuations of the thickness of the muon disk. This finding may indicate a general underestimation of fluctuations of the EAS development by the (CORSIKA) simulations.

(4) The dependence of the EAS time profile from the energy (N_μ^{tr}) and the zenith angle appears to be weak, but significant (especially at larger R_μ). We observe a tendency that the shower disk get less curved and thinner with rising primary energy.

The present studies are focussed to explore phenomenological features of the temporal structure

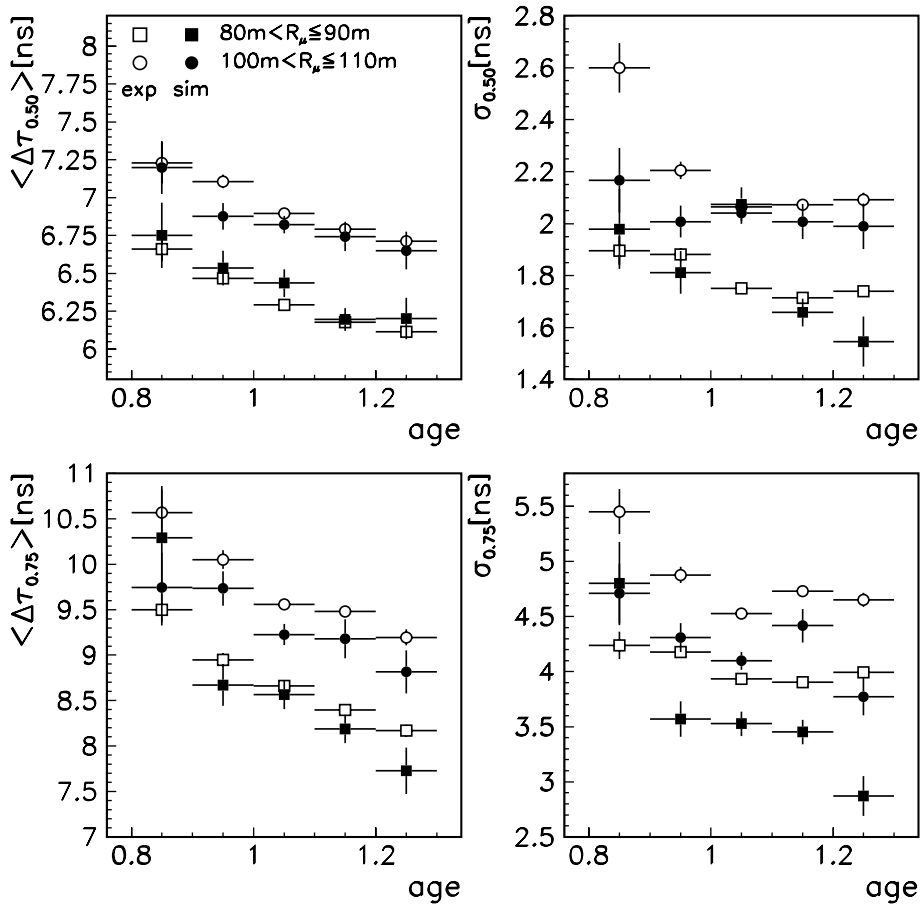

Fig. 12. Age dependence of the average values and their uncertainties of the experimental and simulated median and third-quartile distributions observed at two different ranges of the distance from the shower core ($5° < \theta \leqslant 30°$).

of the EAS muon component, with the question to which extent Monte Carlo simulations do reproduce the observations. The experimental results are a basis for further analyses and interpretations, exploring in multivariate analyses the sensitivity to various different hadronic interaction models (used as generators of the Monte Carlo calculations) or to the mass composition of primary cosmic rays.

Acknowledgements

We acknowledge the clarifying discussions with Prof. Dr. A.A. Watson on the information potential of such investigations. We thank M. Duma for his efficient help in preparing adequate files from the collected data samples for the analysis. We acknowledge the exploratory contributions of Dr. M. Föller and Dr. U. Raidt who participated in an early stage of the investigations. The authors would also like to thank the members of the engineering and technical staff of the KASCADE collaboration who contributed with enthusiasm and engagement to the success of the experiment. The work has been supported by the Ministry for Research of the Federal Government of Germany and, in addition, by a grant of the Romanian National Agency for Science, Research and Technology as well as by a research grant

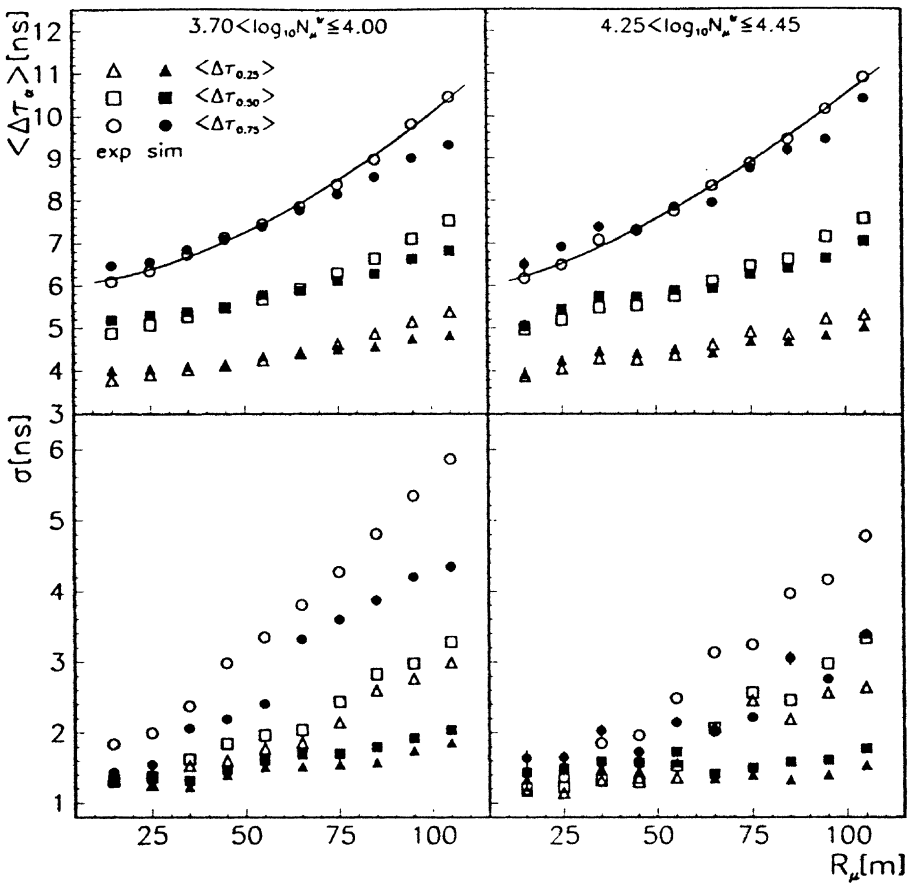

Fig. 13. Experimental and simulated time profiles for two different N_{μ}^{tr} ranges (corresponding to energy ranges of the primary cosmic ray spectrum before and after the "knee") and for $5° < \theta \leqslant 30°$. The simulations adopt a primary mass composition: H:O:Fe = 4:1:2. For the R_{μ}-dependence of $\langle \Delta\tau_{0.75} \rangle$ the results of fits with the quasi-parabolic form (Eq. (6)) are given.

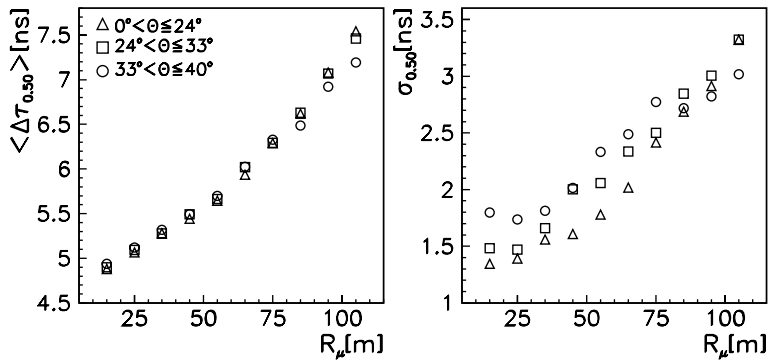

Fig. 14. Experimental time profiles for the median distributions for different angular ranges (equal sec θ – bins) of EAS incidence for $3.6 < \log_{10} N_{\mu}^{tr} \leqslant 4.8$.

(no. 94964) of the Armenian Government and by the ISTC project A116. The collaborating group of the Cosmic Ray Division of the Soltan Institute of Nuclear Studies in Lodz and of the University of Lodz is supported by the Polish State Committee for Scientific Research. The KASCADE collaboration work is embedded in the frame of scientific-technical cooperation (WTZ) projects between Germany and Romania (no. RUM-014-97), Poland (no. 92-94) and Armenia (no. 002-98).

Appendix A. Local time correction procedure

The observed (local) arrival time distributions are a superposition of distributions of different muon multiplicities. This feature combined with the time resolution and detection efficiency of the apparatus, leads to distortions of the true shower profile, which mainly arise from the fluctuations of the registered arrival time of the foremost muon (used as reference for local distributions). The inset of Fig. 15 displays schematically the (global) arrival time distribution and the multiplicity dependence of the mean arrival time of the first muon. Nevertheless comparison of the experimental observations with simulated distributions, taking seriously into account the experimental responses, would be reasonable and could indicate the agreement or disagreement. However, the distortions by the specific response of the particular experimental apparatus, do hamper the comparisons with results of other detector arrays. Thus it appears desirable to display the time profiles as corrected for the multiplicity-dependent fluctuations of the arrival time of the foremost muon and to relate the measured and simulated distributions with a certain, arbitrarily chosen value n_{cal} of the multiplicity. This can be done by invoking EAS simulations using the CORSIKA program. We sketch briefly the procedure of such a "local time correction". The appearance of proton and iron initiated EAS of vertical incidence and of the primary energy $E_0 = 3 \times 10^{15}$ eV has been simulated for the time resolution of 1.7 ns. A sample with a 1:1 mass composition has been considered. The local time correction, which has been estimated for 15 radial ranges R_μ: 0–10 m, 10–20 m, ..., 140–150 m, is practically insensitive to the primary energy and the mass composition. Small influences appear with the variation of the zenith angle of EAS incidence, but for sake of simplicity only EAS of vertical incidence have been taken into account for the present correction procedure. In order to approximate the true shower front, the global arrival time distributions (i.e. relative to the arrival of the light front in the core) have been calculated for all muons (of the chosen energy threshold), cumulating all simulated showers. According to this distribution (taken as estimate of the p.f. of the muon arrival times) for each radial bin n individual arrival times have been randomly selected and the local quartiles (i.e. of distributions relative to the arrival time of the earliest muon) have been calculated. The dependence of the local time quantity from a particular value of n has been generated by repeating the procedure 5000 times. Fig. 15 displays an example: the variation of the observed average median of the local arrival time distributions with the multiplicity, calculated for three different R_μ ranges. Using such curves, $\Delta\tau_\alpha(n)$ observed with the actual multiplicity n can be related to a certain "calibration" value n_{cal}. The

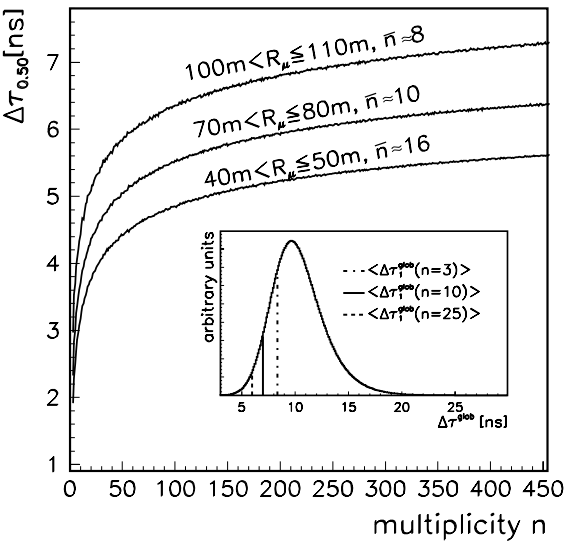

Fig. 15. Multiplicity dependence of the average median of the local arrival time distribution of 2.4 GeV EAS muons registered with the KASCADE central detector. The inset indicates how the expectation values $\langle\Delta\tau_1\rangle$ of the arrival time of the first muon depends on the multiplicity.

difference $\Delta\tau_\alpha(n_{\rm cal}) - \Delta\tau_\alpha(n)$ defines the local time correction. In the present paper we relate the observations and simulations to $n_{\rm cal} = 456$.

References

[1] J. Linsley, L. Scarsi, B. Rossi, Phys. Rev. Lett. 6 (1961) 485.
[2] J. Linsley, L. Scarsi, Phys. Rev. 128 (1962) 2384.
[3] R. Thielert, L. Wiedecke, Z. Phys. 179 (1964) 199.
[4] R. Walker, A.A. Watson, J. Phys. G: Nucl. Phys. 7 (1981) 1297.
[5] R. Walker, A.A. Watson, J. Phys. G: Nucl. Phys. 8 (1982) 1131.
[6] H.E. Dixon, K.E. Turver, Proc. Roy. Soc. London A339 (1974) 171.
[7] G. Agnetta, et al., Astropart. Phys. 6 (1997) 301.
[8] M. Ambrosio, C. Aramo, L. Colesanti, T.V. Danilova, A.D. Erlykin, Astropart. Phys. 7 (1997) 329.
[9] M. Ambrosio, C. Aramo, L. Colesanti, A.D. Erlykin, Astropart. Phys. 11 (1999) 497.
[10] M.L. Armitage, P.R. Blake, W.F. Nash, J. Phys. A: Math. Gen. 8 (1975) 1005.
[11] H. Rebel, G. Völker, M. Föller, A.A. Chilingarian, J. Phys. G: Nucl. Part. Phys. 21 (1995) 451.
[12] H. Rebel, in: W. Tkaczyk (Ed.), The Cosmic Ray Mass Composition, Proc. XV Cracow Summer School of Cosmology, 15–19 July 1996, Uniwersytetu Lodzkiego, Lodz, Poland, 1997, p. 91.
[13] T.V. Danilova, D. Dumora, A.D. Erlykin, J. Procureur, J. Phys. G: Nucl. Part. Phys. 20 (1994) 961.
[14] F. Kakimoto, et al., J. Phys. G: Nucl. Phys. 12 (1986) 131.
[15] P.R. Blake, W.S. Collis, M. Luksys, W.F. Nash, A.J. Sephton, J. Phys. G: Nucl. Part. Phys. 16 (1990) 755.
[16] I.M. Brancus, B. Vulpescu, H. Rebel, M. Duma, A.A. Chilingarian, Astropart. Phys. 7 (1997) 343.
[17] H.O. Klages, et al., KASCADE Collaboration, Nucl. Phys. B Proc. Suppl. 52B (1997) 92.
[18] H.O. Klages, et al., Proc. 25th ICRC, vol. 8, Durban, South Africa, 1997, p. 297.
[19] P. Doll, et al., KfK-Report 4686, Kernforschungszentrum Karlsruhe, 1990.
[20] J.N. Capdevielle, et al., KFK-Report 4998, Kernforschungszentrum Karlsruhe, 1992.
[21] D. Heck, J. Knapp, J.N. Capdevielle, G. Schatz, T. Thouw, FZKA-Report 6019, Forschungszentrum Karlsruhe, 1998.
[22] J. Engler, et al., Nucl. Inst. Meth. A 427 (1999) 528.
[23] H. Bozdog, et al., Nucl. Inst. Meth., in press.
[24] A. Haungs, et al., KASCADE Collaboration, FZKA-Report 6105, Forschungszentrum Karlsruhe, 1998.
[25] M. Brendle, U. Raidt, Nucl. Inst. Meth. A412 (1998) 420.
[26] T. Antoni, et al., KASCADE Collaboration, Astropart. Phys., in press.
[27] J.H. Weber, et al., KASCADE Collaboration 25th ICRC, vol. 6, Durban, South Africa, 1997, p. 153.
[28] R. Glasstetter, et al., KASCADE Collaboration 25th ICRC, vol. 6, Durban, South Africa, 1997, p. 157.
[29] M. Föller, U. Raidt, et al., KASCADE Collaboration 25th ICRC, vol. 6, Durban, South Africa, 1997, p. 149.
[30] Graf, Henning, Stange, Wirlich, Formeln und Tabellen der angewandten mathematischen Statistik, Springer, Berlin-Heidelberg, 1987, p. 27.
[31] I.M. Brancus, et al., KASCADE Collaboration, FZKA-Report 6151, Forschungszentrum Karlsruhe, 1998.
[32] H. Fesefeldt, Report PITHA 85/02, RWTH Aachen, Germany, 1985.
[33] K. Werner, Phys. Rep. 232 (1993) 87.
[34] N.N. Kalmykov, S.S. Ostapchenko, A.I. Pavlov, Nucl. Phys. B Proc. Suppl. 52B (1997) 17.
[35] W.R. Nelson, H. Hiroyama, D.W.O. Rogers, SLAC Report, vol. 265, 1985.
[36] Application Software Group, GEANT-Detector Description and Simulation Tool, CERN, 1993.
[37] E.J. de Villiers, D.J. van der Walt, P.K.F. Grieder, G. van Urk, J. Phys. G: Nucl. Phys. 12 (1986) 547.
[38] R. Haeusler, FZKA-Report 6520, Forschungszentrum Karlsruhe, 2000.
[39] B. Wiebel-Sooth, P.L. Biermann, H. Meyer, Astron. Astrophys. 330 (1998) 389.
[40] A.F. Badea, Internal KASCADE Report, November 1999.
[41] C.P. Woidneck, E. Böhm, J. Phys. A: Math. Gen. 8 (1975) 997.
[42] K.V. Bury, Statistical Models in Applied Science, Wiley, NewYork, 1975, p. 299.
[43] W.T. Eadie, D. Drijard, F.E. James, M. Roos, B. Sadoulet, Statistical Methods in Experimental Physics, North Holland, Amsterdam, The Netherlands, 1971, p. 80.
[44] G. Battistoni, A. Ferrari, M. Carboni, V. Patera, Astropart. Phys. 9 (1998) 277.
[45] H. Leibrock, FZKA-Report 6098, Forschungszentrum Karlsruhe, 1998.
[46] J. Linsley, J. Phys. G: Nucl. Phys 12 (1986) 51.
[47] W. Hafemann, FZKA-Report 6470, Forschungszentrum Karlsruhe, 2000.